

Lateral optical anisotropy of type-II interfaces in the tight-binding approach

E.L. Ivchenko and M.O. Nestoklon*

A.F. Ioffe Physico-Technical Institute, Russian Academy of sciences, St. Petersburg 194021, Russia

We have developed the tight-binding theory to study electronic and optical properties of type-II heterostructures CA/C'A' grown from the zinc-blende semiconductors CA and C'A' along the crystallographic direction [001]. The sp^3s^* nearest-neighbor tight-binding model with allowance for the spin-orbit interaction is used to calculate the energy states and the in-plane linear polarization of the spatially-indirect band-edge photoluminescence of InAs/AlSb and ZnSe/BeTe multi-layered structures. The interface parameters for a pair of the nonstandard planes C-A' or C'-A are considered as fitting variables. A wide range of these parameters are shown to allow Tamm-like hole states localized at the interfaces. The theory leads to giant values of the light polarization in the both type-II heterosystems in agreement with existing experimental findings.

PACS numbers: 73.21.Fg, 78.67.De

I. INTRODUCTION

Experiments on absorption-edge photoluminescence of InAs/AlSb,^{1,2} ZnSe/BeTe^{3,4,5}, CdS/ZnSe⁶ and CdSe/BeTe⁷ multi-layered structures have revealed a giant in-plane optical anisotropy in type-II zinc-blende-lattice nanostructures grown along the [001] crystallographic direction, namely, nonequivalence between the axes $x \parallel [1\bar{1}0]$ and $y \parallel [110]$. In our previous theoretical work⁸ we have shown that the dominating role in the nonequivalence of the in-plane axes is played by the interface bond alignment. In a zinc-blende-lattice bulk semiconductor, say InAs as a representative of III-V compounds or ZnSe as a representative of II-VI compounds, any lattice site is a center of the tetrahedral point symmetry. This means in particular that if the [001] axis is chosen as a horizontal line then, for any anion atom, the right-hand-side bonds always lie in the *same* $\langle 110 \rangle$ -like plane, say the (110) plane, whereas the bonds on the left lie in the perpendicular plane ($1\bar{1}0$). An interface between two materials CA and C'A' lacking common anions and cations, $A \neq A'$, $C \neq C'$, consists of two nonstandard planes containing anions of one material and cations of another material and forming an array C-A' either C'-A of definitely-oriented nonstandard chemical bonds. As a result, the relative contributions of the p_x - and p_y -orbitals to the valence-band function near the interface differ substantially.⁸ It is this difference that leads to the observed remarkable anisotropy for the band-edge, spatially-indirect, radiative processes at the type-II interface in the polarizations $e \parallel x$ and $e \parallel y$. The other interface situated vis-a-vis also induces the in-plane anisotropy. If its chemical bonds are different then the point symmetry of the structure is C_{2v} and the anisotropy is retained. The symmetry of an ideal heterostructure with chemically-identical interfaces is higher than that of a single heterojunction because it contains a mirror rotation about the [001] axis by 90°. In this case the role of the axes [110] and [$1\bar{1}0$] is interchanged for the left- and right-hand-side interfaces, their contributions to the anisotropy cancel each other and these axes become

equivalent. A built-in or external electric field $E \parallel [001]$ breaks the balance and induces the anisotropy.^{3,5} Thus, the polarized spectroscopy may be suggested as an efficient method to get information concerning the chemical bonds, intermixing or reconstruction at the interfaces and the comparative properties of normal and inverted interfaces.

The calculation of the matrix element of optical transition at a type-II interface requires the microscopical knowledge of the electron and hole wave functions near the interface. This information can be obtained in a microscopic consideration within the pseudopotential or tight-binding theories rather than by using the effective-mass approximation or the Kane model. The sp^3 tight-binding theory developed in Ref. 8 is the first attempt to describe the giant lateral anisotropy of type-II interfaces, particularly, of ZnSe/BeTe interfaces. The further efforts are needed to extend the theory including into consideration the spin-orbit splitting of the Γ_{15} bands into Γ_8 and Γ_7 subbands⁹ and additional atomic orbitals, i.e. s^* -orbitals.¹⁰ Moreover, it is quite well established, at least theoretically, that at the heterointerface In-Sb in an InAs/AlSb structure there exist interface, or Tamm-like, states.¹¹ In particular, Shen *et al.*¹² have performed estimations of the localization energy for such states in the tight-binding model neglecting the valence-band spin-orbit splitting in the bulk compositional materials. Clearly, it is intriguing to analyze the interplay between the interface and quantum-confined states in such structures and compare the lateral linear polarization of the photoluminescence due to both kinds of valence-band states. This is the main task of the present work, where we have used the sp^3s^* tight-binding model to calculate the conduction- and valence-band states in type-II heterostructures taking into account the spin-orbit interaction, analyze the polarization properties of band-edge optical matrix elements and obtain the quantitative results for InAs/AlSb and ZnSe/BeTe heterostructures. The preliminary results concerning the interface states in InAs/AlSb heterostructures have been reported in Ref. 13.

The paper is organized as follows. In Sec. II we give a

brief description of the sp^3s^* tight-binding model applied to calculate the conduction- and valence-band states in nanostructures, discuss the time-inversion symmetry of the model and go down the list of tight-binding parameters. Section III contains the derivation of interband matrix elements for the optical transitions with allowance made for the spin-orbit interaction. In Sec. IV we present the results of calculations for InAs/AlSb and ZnSe/BeTe heterosystems including the hole localization at InAs/AlSb interfaces (Sec. III A) and the in-plane linear polarization of the photoluminescence (Secs. III B and III C).

II. TIGHT-BINDING MODEL FORMALISM

First of all we outline a tight-binding theory suitable for the calculation of interband optical transitions on a type-II heterojunction. Let us consider a heterostructure grown along the axis [001]. For the electron states with a zero lateral wave vector, i.e., for the states with $k_x = k_y = 0$, the electron wave function in the tight-binding method is written in the form

$$\psi(\mathbf{r}) = \sum_{n,\alpha} C_n^{(\alpha)} \phi_{n\alpha}(x, y, z - z_n). \quad (1)$$

Here $\phi_{n\alpha}(\mathbf{r})$ are the planar atomic orbitals, α is the orbital state index, n enumerates the atomic planes, anionic for even $n = 2l$ and cationic for odd $n = 2l - 1$, $z_n = na_0/4$ is the position of n th atomic plane, and a_0 is the lattice constant of the face-centered cubic lattice. The planar orbitals are related to the atomic orbitals $\Phi_{n\alpha}(\mathbf{r})$ by

$$\phi_{n\alpha} = \sum_{n_1, n_2} \Phi_{n\alpha}(\mathbf{r} - \mathbf{a}_n - n_1\mathbf{o}_1 - n_2\mathbf{o}_2),$$

where n_1, n_2 are arbitrary integers, $\mathbf{o}_1 = (a_0/2)(1, -1, 0)$, $\mathbf{o}_2 = (a_0/2)(1, 1, 0)$, and \mathbf{a}_n is the position of any atom on the n -th atomic plane.

We use the sp^3s^* tight-binding model taking into account the spin-orbit splitting of the p -states. Hence, for each value of n , the subscript α in $\phi_{n\alpha}$ runs through ten values corresponding to ten states $|\Gamma_6, s\rangle$ ($s = \pm 1/2$), $|\Gamma_8, m\rangle$ ($m = 3/2, 1/2, -1/2, -3/2$), $|\Gamma_7, m\rangle$ ($m = \pm 1/2$), $|\Gamma_6^*, s\rangle$ ($s = \pm 1/2$). These states can be expressed in

terms of s, p and s^* orbitals S, X, Y, Z, S^* as

$$\begin{aligned} |\Gamma_6, 1/2\rangle &= \uparrow S, \quad |\Gamma_6, -1/2\rangle = \downarrow S, \\ |\Gamma_8, 3/2\rangle &= -\uparrow \frac{X + iY}{\sqrt{2}}, \\ |\Gamma_8, 1/2\rangle &= \sqrt{\frac{2}{3}} \uparrow Z - \downarrow \frac{X + iY}{\sqrt{6}}, \\ |\Gamma_8, -1/2\rangle &= \sqrt{\frac{2}{3}} \downarrow Z + \uparrow \frac{X - iY}{\sqrt{6}}, \\ |\Gamma_8, -3/2\rangle &= \downarrow \frac{X - iY}{\sqrt{2}}, \\ |\Gamma_7, 1/2\rangle &= \frac{1}{\sqrt{3}} [\uparrow Z + \downarrow (X + iY)], \\ |\Gamma_7, -1/2\rangle &= \frac{1}{\sqrt{3}} [\downarrow Z - \uparrow (X - iY)], \\ |\Gamma_6^*, 1/2\rangle &= \uparrow S^*, \quad |\Gamma_6^*, -1/2\rangle = \downarrow S^*. \end{aligned} \quad (2)$$

Hereafter the orbitals X and Y as well as the axes x, y are oriented along $[1\bar{1}0]$ and $[110]$, respectively.

In the tight-binding method, the wave equation for an electron with the energy E transforms into a system of linear equations for the coefficients $C_n^{(\alpha)}$, namely,

$$(E_n^{\alpha b} - E) C_n^{(\alpha)} + \frac{1}{2} \sum_{n' \neq n, \alpha'} V_{n\alpha, n'\alpha'} C_{n'}^{(\alpha')} = 0. \quad (3)$$

Here E_n^{α} are the diagonal atomic energies, and $V_{n\alpha, n'\alpha'} = V_{n'\alpha', n\alpha}$ are the off-diagonal matrix elements of tight-binding Hamiltonian for the pair n, n' . In this work we assume the nearest neighbor approximation, where $V_{n\alpha, n'\alpha'} = 0$ for $n \neq n' \pm 1$.

Neglecting the spin-orbit interaction, the sp^3 nearest-neighbor tight-binding Hamiltonian in a homogeneous semiconductor crystal is described by nine parameters $E_{sa}, E_{sc}, E_{pa}, E_{pc}, V_{ss}, V_{xx}, V_{xy}, V_{sa,pc} = V_{pc,sa}$ and $V_{sc,pa} = V_{pa,sc}$.⁸ Note that only in this particular case the notation x, y means the crystallographic axes [100] and [010]. Following Vogl *et al.*¹⁰ we include s^* -orbitals adding four other parameters $E_{s^*a}, E_{s^*c}, V_{s^*a,pc}, V_{s^*c,pa}$ and neglecting the transfer integrals $V_{s^*s^*}, V_{s^*a,sc}, V_{s^*c,sa}$. The spin-orbit splittings Δ_c, Δ_a of the p -orbital cation and anion states complete the list of tight-binding parameters.

Due to the time-inversion symmetry, any electronic state in the heterostructure with $k_x = k_y = 0$ must be doubly degenerate. This is the so-called Kramers degeneracy. It means that if we have a solution of the Schrödinger equation ψ we can obtain the second one, $\bar{\psi}$, by applying the time-inversion operator

$$\bar{\psi} = \hat{K}\psi \equiv i\hat{\sigma}_y\psi^*. \quad (4)$$

In the basis (2), the tight-binding expansion coefficients $C_n^{(\alpha)}, \bar{C}_n^{(\alpha)}$ for the functions ψ and $\bar{\psi}$ are interrelated by

$$\bar{C}_n^{(\alpha)} = \epsilon_\alpha C_n^{(\bar{\alpha})^*}, \quad (5)$$

where the orbitals $\bar{\alpha}$ and α are related by (4), $\epsilon_\alpha = 1$ for the orbitals α with the angular momentum components $s, m = 1/2, -3/2$ and $\epsilon_\alpha = -1$ for α with $s, m = -1/2, 3/2$.

The time-inversion symmetry allows us to separate the states with $k_x = k_y = 0$ into two sets, A and B , one with $C_n^{(\alpha)} = 0$ for $s, m = -1/2, 3/2$ and the other with $C_n^{(\alpha)} = 0$ for $s, m = 1/2, -3/2$. Below we will present explicit equations for $C_n^{(\alpha)}$ for the first set because the states corresponding to the set B are easily obtained by using Eq. (4). Thus, we assume that the wave functions (1) are expanded in the basis

$$|\Gamma_6, 1/2\rangle, |\Gamma_8, -3/2\rangle, |\Gamma_8, 1/2\rangle, |\Gamma_7, 1/2\rangle, |\Gamma_6^*, 1/2\rangle. \quad (6)$$

Presenting the corresponding five coefficients $C_n^{(\alpha)}$ as a five-component column \hat{C}_n we can write the Schrödinger

equation in a matrix form as

$$\begin{aligned} \hat{V}_{2l-1, 2l-2} \hat{C}_{2l-2}^a + (\hat{E}_{2l-1} - E) \hat{C}_{2l-1}^c + \hat{V}_{2l-1, 2l} \hat{C}_{2l}^a &= 0, \\ \hat{V}_{2l, 2l-1} \hat{C}_{2l-1}^c + (\hat{E}_{2l} - E) \hat{C}_{2l}^a + \hat{V}_{2l, 2l+1} \hat{C}_{2l+1}^c &= 0. \end{aligned} \quad (7)$$

For clarity, the symbols \hat{C}_n are supplied with an additional superscript a for anions (even n) and c for cations (odd n). Other notations used are as follows: \hat{E}_n is a diagonal 5×5 matrix with the components $E_{sc}, E_{pc} + \Delta_c/3, E_{pc} + \Delta_c/3, E_{pc} - 2\Delta_c/3, E_{s^*c}$ if $n = 2l - 1$ and $E_{sa}, E_{pa} + \Delta_a/3, E_{pa} + \Delta_a/3, E_{pa} - 2\Delta_a/3, E_{s^*a}$ if $n = 2l$; $\{\hat{V}_{n, n'}\}_{\alpha, \alpha'}$ are 5×5 matrices of tight-binding cation-anion transfer integrals $V_{n\alpha, n'\alpha'}$. In particular, the matrix $\hat{V}_{2l-1, 2l}$ is given by

$$\hat{V}_{2l-1, 2l} = \frac{1}{2} \begin{bmatrix} V_{ss} & 0 & \eta V_{sc, pa} & \xi V_{sc, pa} & 0 \\ 0 & V_{xx} & -\xi V_{xy} & \eta V_{xy} & 0 \\ -\eta V_{sa, pc} & -\xi V_{xy} & V_{xx} & 0 & -\eta V_{s^*a, pc} \\ -\xi V_{sa, pc} & \eta V_{xy} & 0 & V_{xx} & -\xi V_{s^*a, pc} \\ 0 & 0 & \eta V_{s^*c, pa} & \xi V_{s^*c, pa} & 0 \end{bmatrix}, \quad (8)$$

where $\eta = \sqrt{2/3}$, $\xi = \sqrt{1/3}$. The remaining matrices can be obtained from (8) taking into account the symmetry and hermicity of the tight-binding Hamiltonian

$$\begin{aligned} \{\hat{V}_{2l-1, 2l-2}\}_{\alpha, \alpha'} &= (1 - 2\delta_{\alpha, \alpha'}) \{\hat{V}_{2l-1, 2l}\}_{\alpha, \alpha'}, \\ \{\hat{V}_{2l, 2l-1}\}_{\alpha, \alpha'} &= \{\hat{V}_{2l-1, 2l}\}_{\alpha', \alpha}, \\ \{\hat{V}_{2l, 2l+1}\}_{\alpha, \alpha'} &= (1 - 2\delta_{\alpha, \alpha'}) \{\hat{V}_{2l-1, 2l}\}_{\alpha', \alpha}. \end{aligned} \quad (9)$$

A. Energy dispersion in a bulk homogeneous semiconductor

In a three-dimensional semiconductor crystal, the tight-binding coefficients representing the Bloch solutions with the electron wave vector $\mathbf{k} \parallel [001]$ are written as

$$\hat{C}_n^a = \hat{C}_a e^{in\phi}, \quad \hat{C}_n^c = \hat{C}_c e^{in\phi}. \quad (10)$$

Here $\phi = ka_0/4$, \hat{C}_a and \hat{C}_c are independent of n and satisfy the matrix equations

$$(\hat{E}_a - E)\hat{C}_a + \hat{U}_a\hat{C}_c = 0, \quad \hat{U}_c\hat{C}_a + (\hat{E}_c - E)\hat{C}_c = 0, \quad (11)$$

$$\hat{U}_a = \hat{U}_c^\dagger = e^{-i\phi}\hat{V}_{0, -1} + e^{i\phi}\hat{V}_{0, 1}.$$

We took into account that in a periodic system the matrices $\hat{E}_{2l}, \hat{E}_{2l+1}, \hat{V}_{2l, 2l\pm 1}$ etc. are independent of l . Thus, the electron dispersion is determined from a secular 10×10 equation.

B. Application to nanostructures

In the following we consider a type-II heterostructure grown along the axis [001] and consisting of alternating layers of binary compounds CA and C'A' with different cations and anions. We assume the conduction-band bottom to be lower in the CA material and the valence-band top higher in the C'A' material (Fig. 1). The layers are thick enough in order to neglect the formation of superlattice minibands. Thus, the conduction-band states $\psi_c(\mathbf{r})$ are approximately calculated for a single CA layer sandwiched between semiinfinite C'A' layers. In the actual computation procedure the C'A'-layer thicknesses are taken finite but large enough to have ψ_c independent on their size and the external boundary conditions. Similarly, the valence-band states $\psi_v(\mathbf{r})$ are found for the double-interface structure CA/C'A'/CA with thick enough CA layers. By choosing an appropriate set of the tight-binding parameters for all atoms in an InAs/AlAs or ZnSe/BeTe structure, see the details below, and using the standard linear algebra package¹⁴ we can solve Eqs. (7) and obtain both conduction- and valence-band tight-binding states. Then we calculate the optical matrix element due to the indirect photoexcitation $\psi_v \rightarrow \psi_c$ or radiative recombination $\psi_c \rightarrow \psi_v$ at the CA/C'A' interface of the periodic heterostructure with ψ_c being mostly confined within the CA layer and ψ_v confined within the neighboring C'A' layer, as shown by bell-

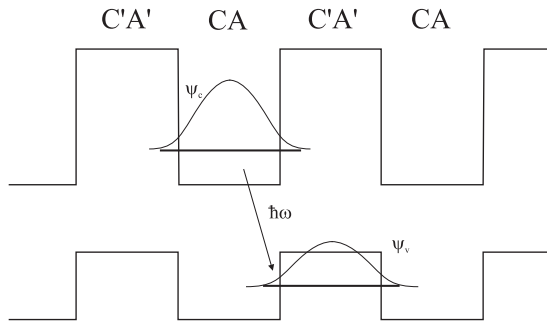


FIG. 1: Band diagram of a type-II heterostructure consisting of the alternating CA and C'A' layers. The higher and lower broken lines show the coordinate dependence of the conduction-band bottom and the valence-band top in the direction of the growth direction z . The arrow illustrates the spatially-indirect optical transition.

shaped curves in Fig. 1.

C. Choice of tight-binding parameters

The chosen sets of tight-binding parameters for bulk InAs, AlSb, ZnSe and BeTe are presented in Table I. For InAs and AlSb, the parameters are taken from the sp^3s^* model of Klimeck *et al.*¹⁵ For bulk ZnSe, the 15 tight-binding parameters of the sp^3s^* model can be borrowed from Refs. 16, 17 and 18. In the main calculation we use the parameters from Ref. 17. The tight-binding parameters for BeTe are the result of our fit of the band-structure data presented in Table II. The band energies at the Γ and X points are calculated by using Eqs. (11), and the effective masses are evaluated by using equations for $m_e, m_{hh}, m_{lh}, m_{so}$ derived in Ref. 19. The parameters evidently differ from those used in Refs. 8 and 20, where the spin-orbit interaction is neglected.

In Table I the diagonal energies refer to the valence-band top, E_{v,Γ_8} , of each bulk material. The diagonal energies E_{ab} used in the calculation for AlSb and BeTe differ from those in the table by the valence band offset V referred to InAs and ZnSe, respectively. In accordance with estimations in Refs. 12,21,22,23 the offset $V \equiv \Delta E_v(\text{InAs} \rightarrow \text{AlSb}) = 0.10$ eV either 0.15 eV is taken for the InAs/AlSb heteropair. For the offset $\Delta E_v(\text{BeTe} \rightarrow \text{ZnSe})$ we use the value 0.95 eV.³

As far as the interface parameters are concerned, for a pair of interface atomic planes C-A' or C'-A we start from the average values $E_{sa}(\text{CA}') = [E_{sa}(\text{A}) + E_{sa}(\text{A}')]/2$, $V_{xx}(\text{CA}') = [V_{xx}(\text{CA}) + V_{xx}(\text{C}'\text{A}')]/2$, etc. Then the sets $E_{ab}(\text{CA}')$ and $E_{ab}(\text{C}'\text{A}')$ are shifted by constant energies in order to satisfy the conditions

$$\begin{aligned} E_{v\Gamma_8}(\text{CA}') - E_{v\Gamma_8}(\text{CA}) &= V'(\text{CA}'), \\ E_{v\Gamma_8}(\text{C}'\text{A}') - E_{v\Gamma_8}(\text{CA}) &= V'(\text{C}'\text{A}'), \end{aligned}$$

where $V'(\text{CA}')$ and $V'(\text{C}'\text{A}')$ are variable parameters of the theory. Shen *et al.*¹² used the value $V'(\text{InSb}) = 0.75$

TABLE I: Tight-binding parameters used in the calculations. The diagonal energies are referred to the Γ_8 valence-band top of the corresponding bulk material.

	InAs	AlSb	ZnSe	BeTe
E_{sa}	-9.57566	-4.55720	-10.19	-9.907
E_{pa}	0.02402	0.01635	0.06	0.58
E_{sc}	-2.21525	-4.11800	0.76	2.04
E_{pc}	4.64241	4.87411	7.22	3.96
E_{s^*a}	7.44461	9.84286	10.0	8.0
E_{s^*c}	4.12648	7.43245	12.0	9.06
V_{ss}	-5.06858	-6.63365	-5.17	-6.00
V_{xx}	0.84908	1.10706	1.22	1.96
V_{xy}	4.68538	4.89960	5.48	5.5
$V_{sa,pc}$	2.51793	4.58724	5.41	-1.0
$V_{sc,pa}$	6.18038	8.53398	6.62	7.5
V_{s^*apc}	3.79662	7.38446	5.63	2.8
V_{s^*cpa}	2.45537	6.29608	5.75	5.5
Δ_a	0.38159	0.70373	0.43	1.1
Δ_c	0.37518	0.03062	0.038	0.26

eV while the first-principles all-electron band structure method gives $V'(\text{InSb}) = 0.50$ eV.²³ In this paper we do not confine ourselves to a particular value of $V'(\text{InSb})$ and assume it to lie in the range $0.1 \div 0.75$ eV. As for the offset $V'(\text{ZnTe})$, we used in our calculation three different values 0.5, 0.75 and 1.0 eV bearing in mind that Wei and Zunger²³ obtained $V'(\text{ZnTe}) = 0.73$ eV. In fact, the bulk semiconductors InAs and AlSb (or ZnSe and BeTe) have very close lattice constants which differ remarkably from the lattice constant of bulk InSb (or ZnTe). Due to this lattice mismatch, the InSb and ZnTe interface atomic planes are strongly strained and the related parameters should be quite different from those of unstrained bulk InSb and ZnTe. We take this uncertainty into account by considering the interface off-diagonal matrix element V_{xy} as an additional variable parameter.

TABLE II: The band edges referred to the Γ_8 valence-band top and effective masses of BeTe given in literature (target) and calculated by using the tight-binding (TB) parameters of Table I.

	BeTe TB	BeTe target		BeTe TB	BeTe target ^a
Γ_6^c	4.53	4.53 ^a	m_e	-0.04	< 0
Γ_7^v	-0.96	-0.96 ^a	m_{hh}	0.34	0.34
Γ_7^c	4.6	4.64 ^b	m_{lh}	0.24	0.23
Γ_8^c	5.0	4.99 ^b	m_{so}	0.33	0.40
X_6^c	2.6	2.7 ^a			

^aRef.²⁴

^bRef.²⁵

III. INTERBAND MATRIX ELEMENT OF THE OPTICAL TRANSITION

The matrix element of the optical transition for the photon polarization \mathbf{e} is proportional to the matrix element of the scalar product of the velocity operator and \mathbf{e} . In order to express the matrix elements in terms of the expansion of ψ in planar orbitals, we must first express the velocity operator in the basis of atomic orbitals. The atomic sites are completely determined by the position of the atom $\mathbf{R} = \mathbf{a} + \boldsymbol{\tau}_b$ specified by the location of an elementary cell, \mathbf{a} , and the location $\boldsymbol{\tau}_b$ of the b atom within the cell. Then the tight-binding Hamiltonian is determined by the matrix elements $H_{\alpha'\alpha}(\mathbf{R}', \mathbf{R})$.

The expression for matrix elements of the velocity operator can be found by using the relation

$$\hat{\mathbf{v}} = \frac{i}{\hbar}(H\mathbf{r} - \mathbf{r}H) \quad (12)$$

between the velocity and coordinate operators, taking the Hamiltonian H in the form $H_{\alpha'\alpha}(\mathbf{R}', \mathbf{R})$ and introducing the matrix elements of the coordinate operator $\mathbf{r}_{\alpha'\alpha}(\mathbf{R}', \mathbf{R})$. As a rule, only intrasite matrix elements

$$\mathbf{r}_{\alpha'\alpha}(\mathbf{R}', \mathbf{R}) = (\mathbf{R} \delta_{\alpha'\alpha} + \mathbf{r}_{\alpha'\alpha}) \delta_{\mathbf{R}', \mathbf{R}} \quad (13)$$

are taken into account, see Refs. 26 and 27 and the bibliography therein, where the contribution

$$\mathbf{r}_{\alpha'\alpha} = \langle \mathbf{R}, \alpha' | \mathbf{r} - \mathbf{R} | \mathbf{R}, \alpha \rangle$$

describes inter-orbital transitions within a single atomic site. Here we use the theory developed in Ref. 28 where $\mathbf{r}_{\alpha'\alpha}$ are assumed to vanish and the optical transitions are uniquely determined by the tight-binding parameters. Then, one obtains for the velocity operator

$$\mathbf{v}_{\alpha'\alpha}(\mathbf{R}', \mathbf{R}) = \frac{i}{\hbar} (\mathbf{R} - \mathbf{R}') H_{\alpha'\alpha}(\mathbf{R}', \mathbf{R}).$$

It is seen that, according to this theory, the intra-atomic terms are equal to zero, and the inter-atomic terms are directed along the vector $\mathbf{R} - \mathbf{R}'$, i.e., along the chemical bond between the atoms \mathbf{R} and \mathbf{R}' . In this case, the inter-atomic transitions between the planes $2l, 2l - 1$ and $2l, 2l + 1$ cause the emission of photons polarized in the x and y directions, respectively.

In the sp^3 tight-binding approach without spin-orbit interaction an expression for interband matrix element of the optical transition is⁸

$$M_j = i \frac{a_0}{4\hbar} \sum_l V_l^j, \quad (14)$$

$$\begin{aligned} V_l^x &= V_{sa,pc} C_{2l}^{sa*} C_{2l-1}^{p_x c} + V_{pa,sc} C_{2l-1}^{sc*} C_{2l}^{p_x a} - V_{xy} (C_{2l}^{p_z a*} C_{2l-1}^{p_x c} - C_{2l-1}^{p_z c*} C_{2l}^{p_x a}), \\ V_l^y &= V_{sa,pc} C_{2l}^{sa*} C_{2l+1}^{p_y c} + V_{pa,sc} C_{2l+1}^{sc*} C_{2l}^{p_y a} + V_{xy} (C_{2l}^{p_z a*} C_{2l+1}^{p_y c} - C_{2l+1}^{p_z c*} C_{2l}^{p_y a}). \end{aligned}$$

Here M_j is the interband matrix element of the velocity operator \hat{v}_j ($j = x, y$), V_l^x is the contribution to M_x from inter-atomic transitions between the anion plane $2l$ and the cation plane $2l - 1$, V_l^y is a similar contribution to M_y from the $2l$ and $2l + 1$ planes, C_n^{sb} and $C_n^{p_z b}$ are the coefficients describing the admixture of s - and p_z -orbitals in the expansion (1) for an electron state in the lowest conduction band Γ_1 , $C_n^{p_j b}$ are the p_j -orbital coefficients for the hole states in the valence band, $V_{sa,pc}$, $V_{pa,sc}$ and V_{xy} are the above anion-cation transfer integrals. It should be mentioned that Eq. (14) describes the photon absorption. The emission matrix elements are obtained by the complex conjugation of M_j .

The spin-orbit interaction included, one has to consider four interband optical transitions $v, A \rightarrow c, A$, $v, B \rightarrow c, B$, $v, A \rightarrow c, B$ and $v, B \rightarrow c, A$ for each pair of the conduction (c) and valence (v) subbands, where

A, B denote the Kramers-conjugate sets of states. In the polarization $\mathbf{e} \perp z$ the first two transitions are forbidden while the absolute values of the matrix elements for the two latter transitions coincide. Hence, it suffices to present an equation only for the $v, B \rightarrow c, A$ matrix element. For $\mathbf{e} \parallel x$ and $\mathbf{e} \parallel y$, it reads, respectively,

$$V_l^x = \hat{C}_{2l-1}^{c,A\dagger} \hat{V}_{x1} \hat{C}_{2l}^{v,B} + \hat{C}_{2l}^{c,A\dagger} \hat{V}_{x2} \hat{C}_{2l-1}^{v,B}, \quad (15)$$

$$V_l^y = \hat{C}_{2l+1}^{c,A\dagger} \hat{V}_{y1} \hat{C}_{2l}^{v,B} + \hat{C}_{2l}^{c,A\dagger} \hat{V}_{y2} \hat{C}_{2l+1}^{v,B}.$$

Five coefficients $C_n^{(\alpha)}$ for the initial valence and final conduction states are represented here by five-component columns $\hat{C}_n^{v,B}$ and $\hat{C}_n^{c,A}$. The matrices \hat{V}_{x1} , \hat{V}_{y1} are given by

$$\hat{V}_{x1} = \frac{1}{\sqrt{2}} \begin{bmatrix} 0 & -V_{sc,pa} & \xi V_{sc,pa} & -\eta V_{sc,pa} & 0 \\ -V_{sa,pc} & 0 & \eta V_{xy} & \xi V_{xy} & -V_{s^*a,pc} \\ \xi V_{sa,pc} & -\eta V_{xy} & 0 & -V_{xy} & \xi V_{s^*a,pc} \\ -\eta V_{sa,pc} & -\xi V_{xy} & V_{xy} & 0 & -\eta V_{s^*a,pc} \\ 0 & -V_{s^*c,pa} & \xi V_{s^*c,pa} & -\eta V_{s^*c,pa} & 0 \end{bmatrix}, \quad (16)$$

$$\hat{V}_{y1} = \frac{i}{\sqrt{2}} \begin{bmatrix} 0 & -V_{sc,pa} & -\xi V_{sc,pa} & \eta V_{sc,pa} & 0 \\ -V_{sa,pc} & 0 & -\eta V_{xy} & -\xi V_{xy} & -V_{s^*a,pc} \\ -\xi V_{sa,pc} & \eta V_{xy} & 0 & -V_{xy} & -\xi V_{s^*a,pc} \\ \eta V_{sa,pc} & \xi V_{xy} & V_{xy} & 0 & \eta V_{s^*a,pc} \\ 0 & -V_{s^*c,pa} & -\xi V_{s^*c,pa} & \eta V_{s^*c,pa} & 0 \end{bmatrix}, \quad (17)$$

while the two other matrices are obtained by the transposition, namely, $\hat{V}_{x2} = \hat{V}_{x1}^\dagger$, $\hat{V}_{y2} = \hat{V}_{y1}^\dagger$.

In the polarization $\mathbf{e} \parallel z$, for the chosen sets of states the inter-set optical transitions $A \leftrightarrow B$ are forbidden while the transitions $v, A \rightarrow c, A$ and $v, B \rightarrow c, B$ have equal probability rates. For the sake of brevity we omit an expression for M_z similar to Eqs. (14, 15).

IV. RESULTS AND DISCUSSION

Conduction- and valence-band states have been calculated with the aid of an original computer program using cLapack¹⁴ which allows to solve the equation set (7). Interface states are identified as those with energies lying above the valence band top of the $C'A'$ material and below the conduction band bottom of the CA material, see Fig. 1. As mentioned above, each calculation was performed for a CA (or $C'A'$) layer of finite thickness L sandwiched between thick layers $C'A'$ (or CA) so that both interface and quantum-confined states could be calculated simultaneously. The localization energy at a single heterointerface could be found as a nonzero limit of the localization energy with increasing the width L . In contrast, the energy of quantum-confined states tends to zero as L^{-2} .

A. Hole localization at InAs/AlSb interfaces

Figures 2 and 3 present our tight-binding calculations of the two lowest hole states in a three-layer structure InAs/AlSb/InAs with the InSb-like interfaces and a 60-Å-thick AlSb layer (40 monoatomic layers, or 20 monomolecular layers). For the InAs/AlSb valence band offset V , we took 0.1 eV. We define the localization energy ε of a hole state as the difference between the energy E (in the electron representation) and the AlSb valence-band top, as shown in the inset in Fig. 2. Therefore,

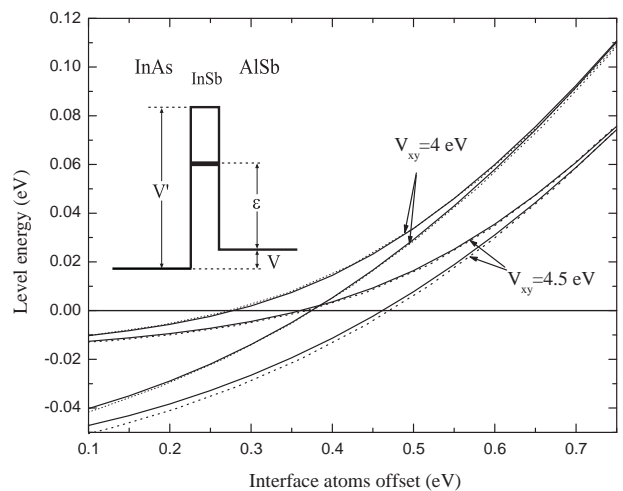


FIG. 2: Localization energy for symmetrical and antisymmetrical interface hole states in an InAs/AlSb multilayered structure with the In-Sb interfacial bonds vs. InSb valence-band offset, V' , for two different values of the interface off-diagonal tight-binding parameter $V_{xy} = 4.0$ eV and 4.5 eV (solid curves). Dotted curves represent analytic results in the envelope-function approximation with a δ -like interface potential. The inset shows the effective band diagram of the InSb-like interface.

values of ε are positive for hole interface states and negative for states quantum-confined within the whole AlSb layer. One can see from Figs. 2, 3 that there exists a wide range of interface parameters allowing interface, or Tamm-like, hole states. The analysis shows that V_{xy} and V' are those two parameters which have the strongest influence on ε . Variation of the diagonal energies $E_{\alpha b}$ and the transfer integrals V_{ss} , V_{pp} also changes the level position. However, these parameters affect the localization energy mostly through a change of the InSb valence-band offset induced by their variation. This explains why we show in Figs. 2 and 3 the dependence of ε upon V' and V_{xy} keeping other parameters constant.

To interpret the results physically, we have applied the envelope-function approximation and simulated the interface localization by a single-quantum-well structure of the thickness L with a band offset V and a pair of δ -functions of equal strength at the interfaces. Thus, the hole potential energy $V(z)$ as a function of z is assumed to have the form

$$V\theta\left(|z| - \frac{L}{2}\right) - Ua_0\left[\delta\left(z - \frac{L}{2}\right) + \delta\left(z + \frac{L}{2}\right)\right],$$

where $\theta(x)$ is the Heaviside step function, the origin $z = 0$ is chosen in the well center, and the lattice constant a_0 is introduced in order to have the energy units for the factor U . In the following we take $a_0 = 6.08 \text{ \AA}$. Obviously, interface states with $\varepsilon > 0$ can exist if U is positive and exceeds some critical value. Two other model parameters are the heavy-hole effective masses m_1 and m_2 in bulk AlSb and InAs, respectively. Their values are taken from our tight-binding estimations for the bulk compositional materials. It should be noted (see, e.g., Ref. 29) that, in the effective-mass approximation, the role of the above δ -like potential is equivalent to the inclusion of an additional term proportional to U in the boundary conditions for the hole envelope function $\varphi(z)$, namely,

$$\varphi_1\left(\pm\frac{L}{2}\right) = \varphi_2\left(\pm\frac{L}{2}\right) \equiv \varphi\left(\pm\frac{L}{2}\right),$$

$$\frac{1}{m_1}\varphi_1'\left(\pm\frac{L}{2}\right) = \frac{1}{m_2}\varphi_2'\left(\pm\frac{L}{2}\right) \pm \frac{2Ua_0}{\hbar^2}\varphi\left(\pm\frac{L}{2}\right).$$

Here the subscripts 1 and 2 denote for short the materials InAs and AlSb.

Due to the inversion symmetry of the potential energy $V(z)$, the functions $\varphi(z)$ have a definite parity. For the interface states, the even or odd solutions can be written in the form $C \cosh(\varkappa z)$ or $C \sinh(\varkappa z)$ inside the well, and

$$C \cosh\left(\frac{\varkappa L}{2}\right) \exp\left[-\varkappa'\left(|z| - \frac{L}{2}\right)\right]$$

or

$$C \text{sign}\{z\} \sinh\left(\frac{\varkappa L}{2}\right) \exp\left[-\varkappa'\left(|z| - \frac{L}{2}\right)\right]$$

in the barriers, where

$$\varkappa = \sqrt{2m_1\varepsilon/\hbar^2}, \quad \varkappa' = \sqrt{2m_2(\varepsilon + V)/\hbar^2}, \quad (18)$$

and C is the normalization coefficient. The localization energy ε satisfies the following transcendental equations

$$\begin{aligned} \varkappa'[1 + \eta \tanh(\varkappa L/2)] &= \beta \quad (\text{for even solution}) \\ \varkappa'[1 + \eta \coth(\varkappa L/2)] &= \beta \quad (\text{for odd solution}), \end{aligned} \quad (19)$$

where $\eta = (m_1\varkappa/m_2\varkappa')$, $\beta = 2m_2a_0U/\hbar^2$.

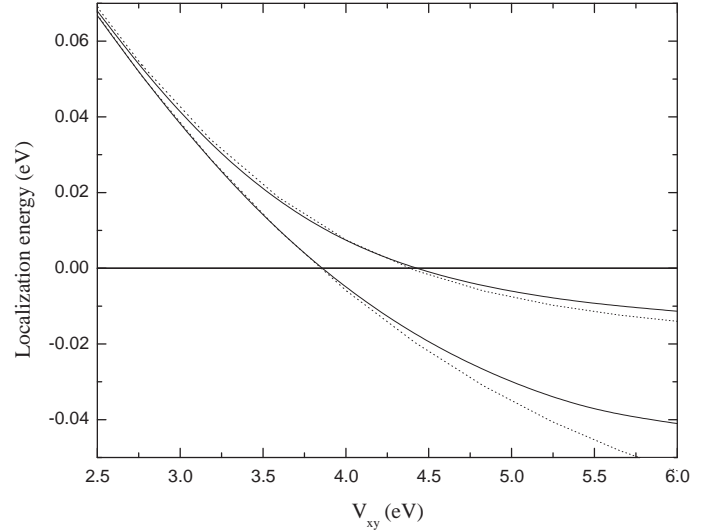


FIG. 3: Localization energy for the hole interface states as a function of interfacial tight-binding parameter V_{xy} . Interface-atom valence-band offset V' is 0.35 eV (solid curves). Dotted curves are analytic results obtained in the envelope-function approximation with a δ -like interface potential.

In the particular case of zero offset and equal effective masses, Eqs. (19) reduce to those for the simple one-dimensional model of a diatomic molecule.³⁰ For very wide wells, $\tanh(\varkappa L/2)$, $\coth(\varkappa L/2) \rightarrow 1$ and Eqs. (19) turn into the equation

$$\varkappa'(1 + \eta) = \beta$$

for the hole interface states at a single heterointerface. For small values of $\exp(-\varkappa L)$, the even-odd splitting can be estimated as

$$\delta\varepsilon = \frac{8\varepsilon_0\varkappa'_0}{\varkappa'_0 + \varkappa_0} \exp(-\varkappa_0 L), \quad (20)$$

where the subscript 0 refers to the values of ε , \varkappa , \varkappa' related to a single-interface state.

We have tried to fit the tight-binding curves in Figs. 2 and 3 by choosing a particular form of dependence of U on V' and V_{xy} . For simplicity, we have assumed the linear dependence

$$U = U_0 + c_1V' + c_2V_{xy}, \quad (21)$$

where U_0 , c_1 , c_2 are fitting parameters. Surprisingly, this simple assumption has proved to work. The dotted curves in Figs. 2, 3 represent the results obtained in the envelope-function approach by using the following set: $U_0 = 26.99 \text{ eV}$, $c_1 = 33.55$, $c_2 = -6.36$. One can see that this approach successfully simulates the behavior of two lowest hole states in the wide range of V' and V_{xy} . For $V' = 0.35 \text{ eV}$ and $V_{xy} = 4 \text{ eV}$, the simplified exponential description of the even-odd splitting by Eq. (20) is certainly justified in the structures with the layer thickness L exceeding 60 \AA provided $\varepsilon_0 \gtrsim 0.015 \text{ eV}$.

An increase in V_{xy} or a decrease in V' lowers the effective interface potential and transforms the pair of interface hole states into the two lowest quantum-confined hole states with negative ε . Within a certain two-dimensional area of V_{xy} and V' the values of ε for the even and odd states have opposite signs. This is a transitional area from the interface localization to quantum confinement. In this case it is possible that, in a wide well, interface states are absent while, with decreasing L , there appears an even interface-induced state with $\varepsilon > 0$ which is, in fact, not attached to the interfaces but rather spread over the whole AlSb layer. In other words, the existence of a hole state inside the bandgap of the heterostructure can depend not only on interface properties but also on the well width L .

Since $|c_2| \ll c_1$ we conclude that, as compared with V_{xy} , the offset V' has the much stronger influence on the localization energy. On the other hand, the parameter V_{xy} plays a more crucial role in the polarization properties of the vertical band-edge photoluminescence, as will be seen in the next section. Thus, the above analysis is a clear and unambiguous indication that the two hole states with $\varepsilon > 0$ represented in Figs. 2, 3 are admixtures of the left- and right-hand-side interface states.

Of course, the symmetry analysis can be applied as well to the tight-binding Hamiltonian and tight-binding solutions. A (001)-grown InAs/AlSb/InAs structure with the symmetrical InSb-like interfaces has the D_{2d} point symmetry with the center O of the point transformations located at any atomic site in the central cation plane n_0 . We recall that the D_{2d} group contains a mirror-rotation axis S_4 . The two lowest hole states of Figs. 2, 3 have a heavy-hole-like nature with an admixture of light-hole, spin-orbit-split and conduction-band states. Therefore, the parity $p = \pm$ of the envelope function $\varphi(z)$ with respect to the operation S_4 coincides with that of the coefficients $C_n^{(\Gamma_8, -3/2)}$ or $C_n^{(\Gamma_8, 3/2)}$ in the expansion (1) over the A or B basis set, namely,

$$C_{n-n_0}^{(\Gamma_8, \pm 3/2)} = p C_{n_0-n}^{(\Gamma_8, \pm 3/2)}. \quad (22)$$

The coefficients $C_n^{(\Gamma_6, \pm 1/2)}$, $C_n^{(\Gamma_6^*, \pm 1/2)}$ behave in the same way whereas the parity of $C_n^{(\Gamma_8, \pm 1/2)}$ and $C_n^{(\Gamma_7, \pm 1/2)}$ is opposite to (22). These symmetry considerations are in a complete agreement with the parities of microscopic solutions obtained in our tight-binding calculations.

An increase in the InAs/AlSb valence-band offset, V , suppresses the localizing effect of the In-Sb interface. The computation shows that, at $V = 0.15$ eV, the lowest valence-band states are pushed out beyond the heterostructure band gap and the energy ε takes on negative values within the relevant range of V' and V_{xy} .

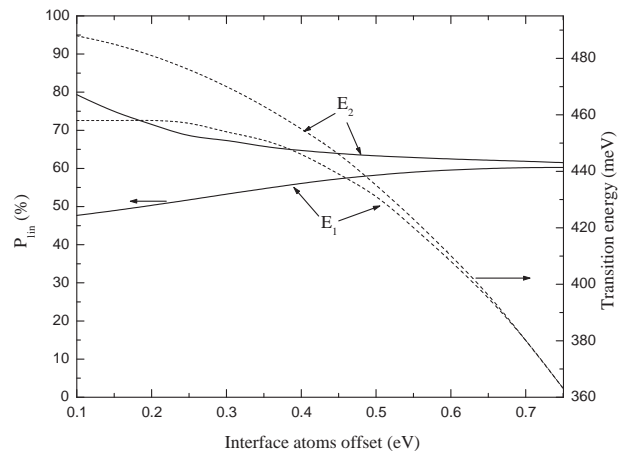


FIG. 4: Transition energy (*dashed*) and linear polarization (*solid*) of the indirect radiative recombination at an 60Å/60Å InAs/AlSb heterointerface as a function of the In-Sb interface atoms valence-band offset V' for the interface off-diagonal tight-binding parameter $V_{xy}=4.0$ eV.

B. Optical properties of InAs/AlSb heterostructures

Figures 4, 5 show the transition energy and in-plane linear polarization of the indirect photoluminescence at a particular interface as functions of the interface parameters V' and V_{xy} . The conduction-band states are calculated for a three-layer structure AlSb/InAs/AlSb with a 60-Å-thick inner InAs layer and the InSb-like interfaces. The transition energies are defined by

$$E_{1,2} = E_g^{(i)} + E_{e1} - \varepsilon_{\pm}, \quad (23)$$

where the indirect band gap $E_g^{(i)}$ equals the difference, $E_{c\Gamma_6}(\text{InAs}) - E_{v\Gamma_8}(\text{AlSb})$, between the the conduction-band bottom in InAs and the valence-band top in AlSb, E_{e1} is the quantum-confinement energy of an electron in the lowest conduction subband $e1$, and ε_{\pm} is the hole localization energy for the even and odd solutions, respectively. The degree of linear polarization is given by

$$P_{\text{lin}} = \frac{|M_x|^2 - |M_y|^2}{|M_x|^2 + |M_y|^2}, \quad (24)$$

where the matrix elements M_x, M_y are introduced in Eq. (14). For their calculation the envelope-function approximation is unusable, and one needs a microscopic description of the X - and Y -orbital admixture in the electron wave function (1).

As compared with ε , the transition energy increases faster with increasing the parameter V' because the latter also affects the electron confinement energy E_{e1} . On the other hand, the energy difference $E_2 - E_1$ of course coincides with $\varepsilon_+ - \varepsilon_-$ as it follows from Eq. (23). One can conclude from Figs. 4, 5 that the linear polarization is very sensitive to the parameter V_{xy} and rather stable

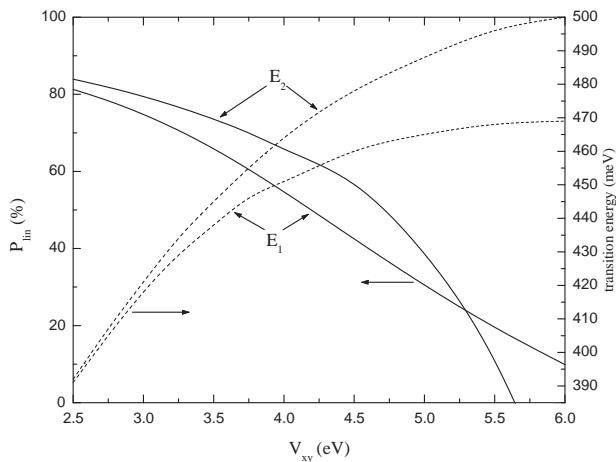


FIG. 5: Transition energy (*dashed*) and linear polarization (*solid*) of indirect radiative-recombination at a $60\text{\AA}/60\text{\AA}$ InAs/AlSb heterointerface as a function of the interface off-diagonal tight-binding parameter V_{xy} . The calculation is performed for the interface-atoms valence-band offset $V' = 0.35$ eV.

to a variation of V' . This is in line with the symmetry considerations. The energy V' is a uniaxial invariant whereas the transfer integral V_{xy} is an interface parameter governing the in-plane anisotropy expressed in a non-equivalence between the $[1\bar{1}0]$ and $[110]$ directions. It should be noted that the same linear polarization is expected for a recombining exciton formed by an electron and hole confined within the neighboring CA and C'A' layers.

Let us now discuss the light polarization taking into account that the radiative process can occur at both normal and inverted interfaces. In an ideal structure of the D_{2d} symmetry, the photons emitted in the two processes have the same energy, and their contributions to the photoluminescence intensity coincide. In this case, as mentioned in the introduction, the linear polarization vanishes, and the information on the optical anisotropy of the individual interface is hidden. If by any reason the photoluminescence intensities I_i , I_n related to the corresponding interface contributions are different, then the observed degree of linear polarization is given by

$$\bar{P}_{\text{lin}} = (2\zeta - 1)P_{\text{lin}}, \quad (25)$$

where $\zeta = I_n/(I_n + I_i)$, and P_{lin} is the linear polarization (24) referred to the normal interface.

Experimental studies of spatially direct and indirect photoluminescence from (001)-grown InAs/AlSb heterostructures are presented by Fuchs *et al.*^{1,2,31} The shutter sequence during the MBE growth promoted InSb-like interfaces which was confirmed via Raman measurements. The polarization-resolved spatially-indirect photoluminescence of all samples showed a strong optical in-plane anisotropy. In particular, this was the case for a multilayered heterostructure that contained two InAs 75-Å-thick layers separated by a 50-Å-thick AlSb layer and

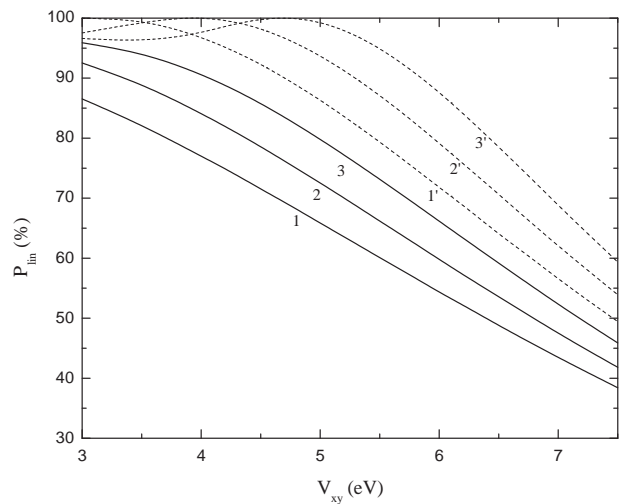


FIG. 6: The linear polarization of spatially-indirect optical transitions at a ZnSe/BeTe heterointerface calculated as a function of the interface off-diagonal tight-binding parameter V_{xy} . The results are presented for the radiative recombination between an electron from the lowest conduction subband $e1$ and a hole from the lowest hole subband (*solid*) and the first excited hole subband (*dashed*). The calculation is performed for three values of interface-atoms offset, $V' = 0.5$ eV (curves 1 and 1'), 0.75 eV (2 and 2') and 1 eV (3 and 3').

surrounded by two other, thick enough, AlSb layers. For the vertical photoluminescence along the growth direction, the linear polarization P_{lin} was as high as $\sim 60\%$. We assume that, in the experiment² the photoluminescence originated from the radiative recombination at one interface, say, due to a slight asymmetry of the heterostructure and a preferential occupation by photoholes of the states at a particular interface. Then according to Figs. 4, 5 our theory explains the measured high values of P_{lin} provided $V_{xy} < 4$ eV for $V' = 0.35$ eV or $V' > 0.5$ for $V_{xy} = 4$ eV.

Now we discuss the intensity I_z of the z -polarized light emitted in the direction x or y perpendicular to z . First of all, we note that the optical transitions involving the heavy-hole states become allowed in the polarization $\mathbf{e} \parallel z$ only due to an admixture of the Z orbitals to these states. Neglecting the spin-orbit interaction, the orbital Z and the orbitals X, Y do not mix in the states with $k_x = k_y = 0$.⁸ For large values of the spin-orbit splitting of the valence band as in the case of AlSb, an admixture of the Z orbitals in the heavy-hole subband appears (i) due to the heavy-light-hole mixing at the interfaces^{32,33} or/and (ii) due to $k_{x,y}$ -induced mixing of the heavy- and light-hole states. Our calculation shows that, for an ideal InAs/AlSb interface, the indirect radiative recombination of an electron and a heavy hole with $k_x = k_y = 0$ in the polarization $\mathbf{e} \parallel z$ is at least by one order of magnitude less intensive than for $\mathbf{e} \perp z$. In Ref. 2, for the light emission along x and y , the photoluminescence intensity I_z was small compared to I_y and exceeded I_x by a factor of ~ 2 . The observed remarkable z -polarized intensity

may be related to the structure imperfections and the light depolarization on leaving the sample in the in-plane directions.

C. Lateral optical anisotropy of ZnSe/BeTe heterostructures

In Ref. 8 we have demonstrated that the simplest sp^3 nearest-neighbor tight-binding model is consistent with the giant linear polarization $P_{\text{lin}} = 70\text{-}80\%$ of the vertical photoluminescence observed in (001)-grown ZnSe/BeTe multilayered heterostructures. Here we have extended the model from sp^3 to sp^3s^* and included the spin-orbit interaction into consideration. The parameters used in the calculation are presented in Sec. II.C except for the interface transfer integral V_{xy} and the interface-atoms offset V' which were considered as variable parameters. In the studied range of these parameters there is no hole interface localization, and even the lowest hole states are quantum-confined within the whole BeTe layer.

Figure 6 depicts the polarization related to the radiative recombination at one particular interface in a 60Å/60Å ZnSe/BeTe structure with the ZnTe-like interfaces. The polarization degree P_{lin} is shown as function of V_{xy} for three different values of V' and for the optical transitions involving the lowest hole subbands. As compared with the InAs/AlSb heteropair (Figs. 4, 5), the values of P_{lin} are higher, and the sensitivity of P_{lin} to the variation of V_{xy} is much weaker. Clearly, there exist a wide two-parametrical area of V_{xy} and V' where the polarization exceeds 80%. As well as in Ref. 8 the polarization sign follows the Zn-Te interface bond direction.

For comparison, we have also performed the calculations for heterostructures with the BeSe interface atoms.

The main result is that, within the studied values of the interface parameters V_{xy} and V' , the polarization P_{lin} can reverse its sign and is not determined completely by the interface bond direction.

V. CONCLUSION

A tight-binding approach has been developed in order to calculate the electronic and optical properties of type-II heterostructures. In agreement with the existing experiments, the theory allows a giant in-plane linear polarization for the photoluminescence of type-II (001)-grown multi-layered structures with no-common cations and anions, such as InAs/AlSb and ZnSe/BeTe. The calculation shows that the high polarization can be found for the radiative recombination involving both the interface and quantum-confined hole states in the InAs/AlSb structures. Among the set of interface tight-binding parameters the most important are the interface-atoms offset V' and the transfer integral V_{xy} , the first controlling the hole localization at an interface and the second controlling the in-plane optical anisotropy. The developed theory can be generalized to calculate the optical anisotropy of type-II quantum-wire and quantum-dot nanostructures⁷ to study the composition and quality of the interfaces therein.

Acknowledgments

This work is financially supported by the RFBR and the programmes of RAS. One of us (M.O.N.) is grateful to the ‘‘Dynasty’’ Foundation — ICFPM.

* Electronic address: nestoklon@coherent.ioffe.ru

¹ F. Fuchs, J. Schmitz, J. D. Ralston, P. Koidl, R. Heintz, and A. Hoffmann, *Superlatt. Microstruct.* **16**, 35 (1994).

² F. Fuchs, J. Schmitz, and N. Herres, *Proc. the 23rd Internat. Conf. on Physics of Semiconductors*, Ed. by M. Scheffler and R. Zimmermann (World Scientific, Singapore) vol. 3, p. 1803 (1996).

³ A. V. Platonov, V. P. Kochereshko, E. L. Ivchenko, G. V. Mikhailov, D. R. Yakovlev, M. Keim, W. Ossau, A. Waag, and G. Landwehr, *Phys. Rev. Lett.* **83**, 3546 (1999).

⁴ D. R. Yakovlev, E. L. Ivchenko, V. P. Kochereshko, A. V. Platonov, S. V. Zaitsev, A. A. Maksimov, I. I. Tartakovskii, V. D. Kulakovskii, W. Ossau, M. Keim, et al., *Phys. Rev. B* **61**, 2421 (2000).

⁵ D. R. Yakovlev, A. V. Platonov, E. L. Ivchenko, V. P. Kochereshko, C. Sas, W. Ossau, L. Hansen, A. Waag, G. Landwehr, and L. W. Molenkamp, *Phys. Rev. Lett.* **88**, 257401 (2002).

⁶ M. Schmidt, M. Grun, S. Petillon, E. Kurtz, and C. Klingshirn, *Appl. Phys. Lett.* **77**, 85 (2000).

⁷ A. A. Toropov, S. V. Sorokin, T. V. Shubina, O. V.

Nekrutkina, D. D. Solnyshkov, S. V. Ivanov, A. Waag, and G. Landwehr, *phys. stat. sol. (a)* **195**, 551 (2003).

⁸ E. L. Ivchenko and M. O. Nestoklon, *JETP* **94**, 644 (2002).

⁹ D. J. Chadi, *Phys. Rev. B* **16**, 790 (1977).

¹⁰ P. Vogl, H. P. Hjalmarson, and J. D. Dow, *J. Phys. Chem. Sol.* **44**, 365 (1983).

¹¹ H. Kroemer, C. Nguyen, and B. Brar, *J. Vac. Sci. Technol. B* **10**, 1769 (1992).

¹² J. Shen, H. Goronkin, J. D. Dow, and S. Y. Ren, *J. Appl. Phys.* **77**, 1577 (1995).

¹³ M. O. Nestoklon, *Proc. 11th Int. Symp. ‘‘Nanostructures: Physics and Technology’’* (St. Petersburg) p. 86 (2003).

¹⁴ E. Anderson, Z. Bai, C. Bischof, S. Blackford, J. Demmel, J. Dongarra, J. Du Croz, A. Greenbaum, S. Hammarling, A. McKenney, et al., *LAPACK Users’ Guide* (Philadelphia, PA, 1999), 3rd ed., ISBN 0-89871-447-8.

¹⁵ G. Klimeck, R. C. Bowen, T. B. Boykin, and T. A. Cwic, *Superlatt. Microstruct.* **27**, 519 (2000).

¹⁶ D. Bertho, D. Boiron, A. Simon, S. Jouanin, and C. Priester, *Phys. Rev. B* **44**, 6118 (1991).

¹⁷ D. Bertho, J.-M. Jancu, and S. Jouanin, *Phys. Rev. B* **48**,

- 2452 (1993).
- ¹⁸ H. Dierks and G. Czycholl, *Z. Phys. B* **99**, 207 (1996).
- ¹⁹ T. B. Boykin, G. Klimeck, R. C. Bowen, and R. Lake, *Phys. Rev. B* **56**, 4102 (1997).
- ²⁰ L. Zhu and L. Zhang, *J. Phys.: Conens. Matter* **9**, 8055 (1997).
- ²¹ A. Nakagawa, H. Kroemer, and J. H. English, *Appl. Phys. Lett.* **54**, 1893 (1989).
- ²² R. G. Dandrea and C. B. Duke, *Appl. Phys. Lett.* **63**, 1795 (1993).
- ²³ S.-H. Wei and A. Zunger, *Appl. Phys. Lett.* **72**, 2011 (1998).
- ²⁴ M. Nagelstrasser, H. Droge, H.-P. Steinruck, F. Fischer, T. Litz, A. Waag, G. Landwehr, A. Fleszar, and W. Hanke, *Phys. Rev. B* **58**, 10394 (1998).
- ²⁵ A. Fleszar, *Phys. Rev. B* **64**, 245204 (2001).
- ²⁶ M. Cruz, M. R. Beltrán, C. Wang, J. Tagüeña-Martinez, and Y. G. Rubo, *Phys. Rev. B* **59**, 15 381 (1999).
- ²⁷ T. G. Pedersen, K. Pedersen, and T. B. Kristensen, *Phys. Rev. B* **63**, 201101 (2001).
- ²⁸ L. C. L. Y. Voon and L. R. Ram-Mohan, *Phys. Rev. B* **47**, 15500 (1993).
- ²⁹ E. E. Takhtamirov and V. A. Volkov, *JETP* **89**, 1000 (1999).
- ³⁰ A. O. E. Animalu, *Intermediate Quantum Theory of Crystalline Solids* (Prentice-Hall, Inc. New Jersey, 1977).
- ³¹ F. Fuchs, J. Schmitz, J. D. Ralston, and P. Koidl, *Phys. Rev. B* **49**, 13638 (1994).
- ³² E. L. Ivchenko, A. Y. Kaminski, and U. Rössler, *Phys. Rev. B* **54**, 5852 (1996).
- ³³ E. L. Ivchenko, A. A. Toropov, and P. Voisin, *Phys. Solid State* **40**, 1748 (1998).